



# Source contributions to the regional distribution of secondary particulate matter in California

Qi Ying, Michael J. Kleeman\*

*Department of Civil and Environmental Engineering, University of California, Davis, One Shields Avenue, Davis, CA 95616, USA*

Received 15 June 2005; received in revised form 6 October 2005; accepted 6 October 2005

## Abstract

Source contributions to PM<sub>2.5</sub> nitrate, sulfate and ammonium ion concentrations in California's San Joaquin Valley (SJV) (4–6 January 1996) and South Coast Air Basin (SoCAB) surrounding Los Angeles (23–25 September 1996) were predicted using a three-dimensional source-oriented Eulerian air quality model. The air quality model tracks the formation of PM<sub>2.5</sub> nitrate, sulfate and ammonium ion from primary particles and precursor gases emitted from different sources through a mathematical simulation of emission, chemical reaction, gas-to-particle conversion, transport and deposition. The observed PM<sub>2.5</sub> nitrate, sulfate and ammonium ion concentrations, and the mass distribution of nitrate, sulfate and ammonium ion as a function of particle size have been successfully reproduced by the model simulation. Approximately 45–57% of the PM<sub>2.5</sub> nitrate and 34–40% of the PM<sub>2.5</sub> ammonium ion in the SJV is formed from precursor gaseous species released from sources upwind of the valley. In the SoCAB, approximately 83% of the PM<sub>2.5</sub> nitrate and 82% of the PM<sub>2.5</sub> ammonium ion is formed from precursor gaseous species released from sources within the air basin. In the SJV, transportation related sources contribute approximately 24–30% of the PM<sub>2.5</sub> nitrate (diesel engines ~13.5–17.0%, catalyst equipped gasoline engines ~10.2–12.8% and non-catalyst equipped gasoline engines ~0.3–0.4%). In the SoCAB, transportation related sources directly contribute to approximately 67% of the PM<sub>2.5</sub> nitrate (diesel engines 34.6%, non-catalyst equipped gasoline engine 4.7% and catalyst equipped gasoline engine 28.1%). PM<sub>2.5</sub> ammonium ion concentrations in the SJV were dominated by area (including animal) NH<sub>3</sub> sources (16.7–25.3%), soil (7.2–10.9%), fertilizer NH<sub>3</sub> sources (11.4–17.3%) and point NH<sub>3</sub> sources (14.3–21.7%). In the SoCAB, ammonium ion is mainly associated with animal sources (28.2%) and catalyst equipped gasoline engines (16.2%). In both regions, the majority of the relatively low PM<sub>2.5</sub> sulfate (<5 μg m<sup>-3</sup>) is associated with upwind sources. Most of the locally generated sulfate is emitted from diesel engines and high-sulfur fuel combustion processes in both modeling domains. Emissions control programs should target the sources listed above to reduce PM<sub>2.5</sub> concentrations.

© 2005 Elsevier Ltd. All rights reserved.

*Keywords:* Source-oriented air quality model; Source apportionment; Secondary particulate matter; Los Angeles; San Joaquin valley

## 1. Introduction

Airborne particulate matter has significant effects on visibility (Eldering and Cass, 1996; Griffing, 1980; Neuburger, 1995; Pilinis, 1989), global climate change (Dickerson et al., 1997; Jacobson, 2000; Lesins et al., 2002) and human health (Dreher and Costa, 2002;

\*Corresponding author. Tel.: +530 752 8386;  
fax: +530 752 7872.

E-mail address: [mjkleeman@ucdavis.edu](mailto:mjkleeman@ucdavis.edu) (M.J. Kleeman).

Ozkaynak et al., 1996). In 1997, the US Environmental Protection Agency created a National Ambient Air Quality Standard (NAAQS) for PM<sub>2.5</sub> (particulate matter with aerodynamic diameter smaller than 2.5 μm). Approximately 59.2 million people in the US live in areas where ambient concentrations exceed the PM<sub>2.5</sub> NAAQS (EPA, 2003b). From 1999 to 2002, primary PM<sub>2.5</sub> emissions decreased by 17% but ambient PM<sub>2.5</sub> concentrations decreased by only 8% (EPA, 2003a). This slow improvement is partly due to the difficulty in correctly identifying the emission sources that contribute to airborne particulate matter. Secondary particulate matter (such as ammonium nitrate and ammonium sulfate) is typically a major component of PM<sub>2.5</sub> concentrations during the times when the NAAQS for particulate matter are exceeded (Christoforou et al., 2000; Hughes et al., 1999; Mysliwiec and Kleeman, 2002; Watson and Chow, 2002). Traditional receptor-oriented statistical models are unable to identify the sources of these secondary pollutants and thus cannot provide effective guidance for emission reduction efforts (Richards et al., 1999).

Source-oriented air quality models have been used in past studies to directly identify source contributions to primary particulate matter (Kleeman and Cass, 2001; Kleeman et al., 1997). Recent advances in these source-oriented air quality models have directly calculated source contributions to both primary and secondary particulate matter concentrations at specific locations (Mysliwiec and Kleeman, 2002). The purpose of the current study is to use an improved 3D Eulerian air quality model to calculate regional source contributions to secondary particulate matter in the South Coast Air Basin (SoCAB) surrounding Los Angeles (23–25 September 1996) and in the San Joaquin Valley (SJV) (4–6 January 1996) in California. Both areas significantly exceed the NAAQS PM<sub>2.5</sub> 24-h average value of 65 μg m<sup>-3</sup> during the study episodes, potentially affecting the health of the 17.6 million people (EPA, 2003b) living in these regions. In the following sections, the formulation of the 3D Eulerian source-oriented air quality model is described and source contributions to secondary particulate matter in the two regions are calculated.

## 2. Background

Receptor-oriented models have been used to identify the important emission sources that contribute to airborne primary particulate mass in both

California's SJV (Chow et al., 1992; Magliano et al., 1999) and the SoCAB (Schauer et al., 1996; Watson et al., 1994). The chemical mass balance (CMB) method uses measured source profiles (the mass abundances of chemical species in source emissions) and measured ambient profiles to quantify PM<sub>2.5</sub> source contributions. The amount of ammonium ion, sulfate, and nitrate in each source profile changes through gas-phase chemical reactions and gas-to-particle conversion processes (Watson and Chow, 2002). The non-linear nature of this transformation makes it difficult to identify the sources of the secondary particulate matter using receptor-oriented models. Watson et al. used an aerosol evolution model to simulate the changes in source profiles from sources to the receptor and used the predicted source profiles in a CMB modeling study (Watson et al., 2002a). However, aerosol evolution models used to predict the aging of source profiles are often overly simplified and do not reflect the real changes of the source profile (Watson et al., 2002b).

Mechanistic air quality models that simulate the atmospheric chemistry and gas-to-particle conversion of inorganic compounds have been used to provide more information about the formation of the secondary particulate matter and its relation to the precursor gases. (Pun and Seigneur, 2001) used a box model to investigate the formation of secondary ammonium nitrate during the 1995 Integrated Monitoring Study (IMS95) for the SJV. They found that nitric acid is the limiting reagent in the formation of PM<sub>2.5</sub> nitrate and a decrease in NO<sub>x</sub> emission may increase PM<sub>2.5</sub> nitrate. Stockwell et al. (2000) used a box model to determine that under the wintertime conditions in the SJV approximately 33% of the emitted NO<sub>x</sub> was converted to PM<sub>2.5</sub> nitrate. These studies, however, do not provide any source contribution information.

Source-oriented mechanistic air quality models can be used to directly apportion primary and secondary airborne particulate matter while accounting for transport, chemical reaction, gas-to-particle conversion, and deposition. Kleeman and Cass (2001) developed a source oriented 3D Eulerian air quality model and applied it to the SoCAB to identify regional sources contributions to primary particulate matter. This source-oriented air quality model has also been successfully used to study the source contributions to primary particulate matter in the SJV (Held et al., 2004). A comparison of the source apportionment of primary particulate matter using the source-oriented air

quality model and the CMB method has been performed for both SJV valley and the SoCAB and excellent agreement was found between the two methods (Held et al., 2005). However, the regional sources of the secondary particulate matter were not identified in these studies. Mysliwicz and Kleeman (2002) developed a source apportionment algorithm that can directly track the particles and precursor gases released from different sources and calculate source contributions to primary and secondary particulate matter at a single receptor site. Ying et al. (2004) used the same approach in a source-oriented 3D Eulerian model to calculate the source contributions to regional visibility impairment in the SoCAB. To the best of the authors' knowledge, there are no other existing studies that give regional source contributions to secondary particulate matter.

### 3. Model description

The source-oriented 3D Eulerian air quality model used in this study to directly calculate the regional source contributions to secondary particulate matter is based on the Eulerian source-oriented air quality model developed by Kleeman and Cass (2001) that tracks the primary particulate matter from different emission sources and the source apportionment algorithm for secondary particulate matter first described by Mysliwicz and Kleeman (2002). Airborne particles and the precursor gases from different sources that form secondary particulate matter are tracked through a complete description of emission, transport, deposition and chemical transformation. Fig. 1 illustrates one possible reaction pathway for the formation of PM<sub>2.5</sub> nitrate ( $\text{NO}_3^-$ ) from two sources with direct NO emissions.  $\text{RO}_2$  represents a peroxy-type radical, and OH represents hydroxyl radical. Fig. 1(a) shows the traditional approach where NO emissions from the two sources are lumped into a single NO species and the PM<sub>2.5</sub> nitrate formation process does not track source contributions. Fig. 1(b) shows the source-oriented approach where the formation of PM<sub>2.5</sub> nitrate from the two NO sources is tracked separately so that the contribution from each emission source to the PM<sub>2.5</sub> nitrate concentration can be calculated. The additive nature of the chemical reactions ensures that the sum of the nitrate formation rates from the two sources equals the rate of formation that would be calculated in the absence of source apportionment calculations. A

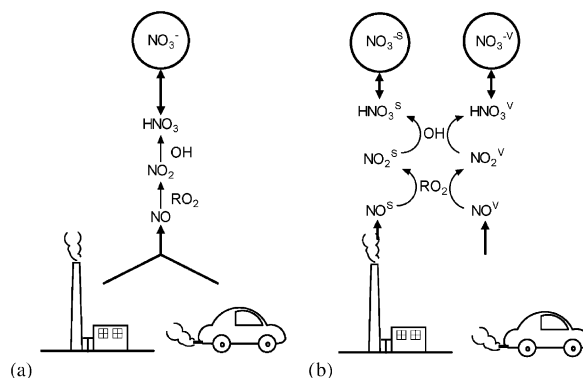


Fig. 1. Illustration of source apportionment for secondary PM<sub>2.5</sub> nitrate from two sources. (a) Formation of secondary PM<sub>2.5</sub> nitrate in traditional air quality model using lumped NO emissions. (b) Formation of secondary PM<sub>2.5</sub> nitrate from NO emitted from two sources tracked separately in the current source-oriented air quality model.

more complete description of the source-oriented 3D Eulerian air quality model and the source apportionment algorithm for secondary particulate matter is provided in Mysliwicz and Kleeman (2002) and Ying et al. (2004).

### 4. Model application

The new 3D source-oriented air quality model with secondary source-apportionment capability has been applied to simulate air quality in the SJV on 4–6 January 1996 and in the SoCAB on 23–25 September 1996. The two episodes represent examples of recent air pollution events in California that have the air quality, meteorology and emission data needed to support the application of a complex 3D Eulerian source-oriented air quality model. Details about the measured concentrations of various gaseous and particulate pollutants for the September SoCAB and January SJV episodes can be found in Kleeman and Cass (2001) and Held et al. (2004), respectively.

Fig. 2 shows the SJV modeling domain in central California and the SoCAB modeling domain in southern California. The major receptor sites for the SJV (Fresno, Kern Wildlife Refuge and Bakersfield) and the SoCAB (Long Beach, Central Los Angeles and Riverside) are indicated on the map. The details of the modeling domain have been described by Kleeman and Cass (2001) and by Held et al. (2004) for the SoCAB and SJV, respectively. In summary, the SJV modeling region is a  $54 \times 72$  rectangular

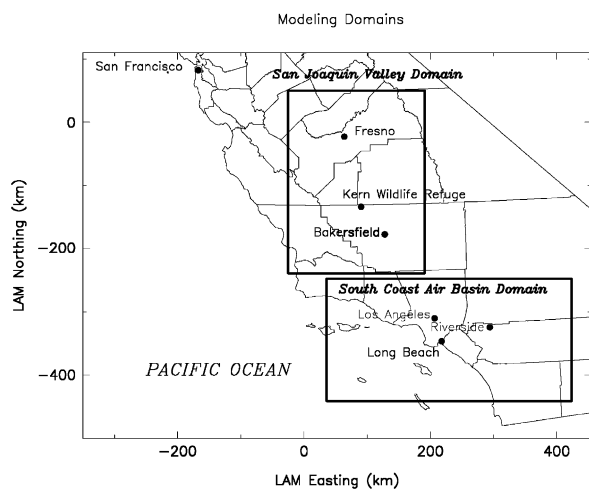


Fig. 2. The SJV and SoCAB air quality modeling domains.

domain with a grid size of 4 km using the Lambert coordinate system. The SoCAB modeling region is an  $80 \times 30$  rectangular domain with a grid size of 5 km using the UTM coordinate system. Five vertical layers with depth of 38.5, 115.5, 154, 363 and 429 m (which gives a total high of 1100 m in the vertical) were used for the SJV modeling domain. The SoCAB domain used 7 layers with depth of 34.5, 65.5, 100, 200, 200, 200, and 200 m (which gives a total thickness of 1000 m). These vertical domains are shallower than the domains that would be needed to model air pollution episodes in the Eastern United States where time scales are longer and spatial domains are larger. In the present study, vertical temperature measurements at sites in the SoCAB and the SJV show that the daytime convective mixing layer seldom reaches 1 km above surface in either domain. The air in the convective surface-mixing layer is essentially decoupled with the layer above. The sensitivity of the model results to the number of vertical layers and the vertical extent of the model domain used to simulate the SoCAB have been studied previously (Ying and Kleeman, 2003) and no significant differences were found when the model domain was extended from 1 to 2 km above surface. Mixing heights in the SJV during the winter period are generally lower than mixing heights in the SoCAB during summer/fall times. Thus it is expected that the 1 km vertical domain used in the current study is sufficient to accurately predict the concentration of pollutants at the ground level. Details of the diagnostic meteorology fields, initial and boundary condition fields

and emission inventories used in the current study can be found in Kleeman and Cass (2001) and Held et al. (2004) and are summarized in the Supplementary Material section of the this paper.

## 5. Model results

### 5.1. Comparison to measurements

Figs. 3(a)–(i) show the observed and predicted time series of PM<sub>2.5</sub> nitrate, ammonium ion and sulfate concentrations on 6 January 1996 for three sites in the SJV. The uncertainty for the observations shown in Fig. 3 are not explicitly known, but they are estimated to be 10–15% based on samples collected in the SJV during a winter air pollution episode (Herner et al., 2005). Fresno and Bakersfield are urban sites influenced by both regional trends and local emissions, while Kern Wildlife Refuge is a rural site located far from major emission sources in the SJV. Figs. 3(a)–(c) show the predicted and observed PM<sub>2.5</sub> nitrate concentration at Fresno, Kern Wildlife Refuge and Bakersfield, respectively. Model predictions agree well with the observations at all three locations. Fig. 3(a) shows that the predicted and observed nitrate concentration at the Fresno site is approximately  $20\text{--}25 \mu\text{g m}^{-3}$ . NO<sub>x</sub> from upwind sources (injected into the SJV from the boundary), diesel engines (in the SJV) and catalyst equipped gasoline engines (in the SJV) are the most significant contributors to PM<sub>2.5</sub> nitrate at this site. Fig. 3(b) shows that there is a significant increase in the PM<sub>2.5</sub> nitrate concentration during the day at the Kern Wildlife Refuge site. The predicted concentration increases from  $13 \mu\text{g m}^{-3}$  in the early morning to over  $30 \mu\text{g m}^{-3}$  in the late afternoon. The observed concentrations follow the general trend, increasing from approximately  $4 \mu\text{g m}^{-3}$  in the early morning to  $22 \mu\text{g m}^{-3}$  in the late afternoon. Likewise, Fig. 3(c) shows that predicted and observed PM<sub>2.5</sub> nitrate concentrations at Bakersfield site both increase from approximately 20 to  $30\text{--}40 \mu\text{g m}^{-3}$  on 6 January 1996. NO<sub>x</sub> released from sources prior to 4 January 1996 (entered in the SJV as an initial condition), diesel engines, catalyst equipped gasoline engines and other anthropogenic sources are the most significant contributors to PM<sub>2.5</sub> nitrate at Kern Wildlife Refuge and Bakersfield on 6 January 1996. Figs. 3(d)–(f) show the predicted and observed PM<sub>2.5</sub> ammonium ion concentrations at Fresno, Kern Wildlife Refuge and Bakersfield, respectively.

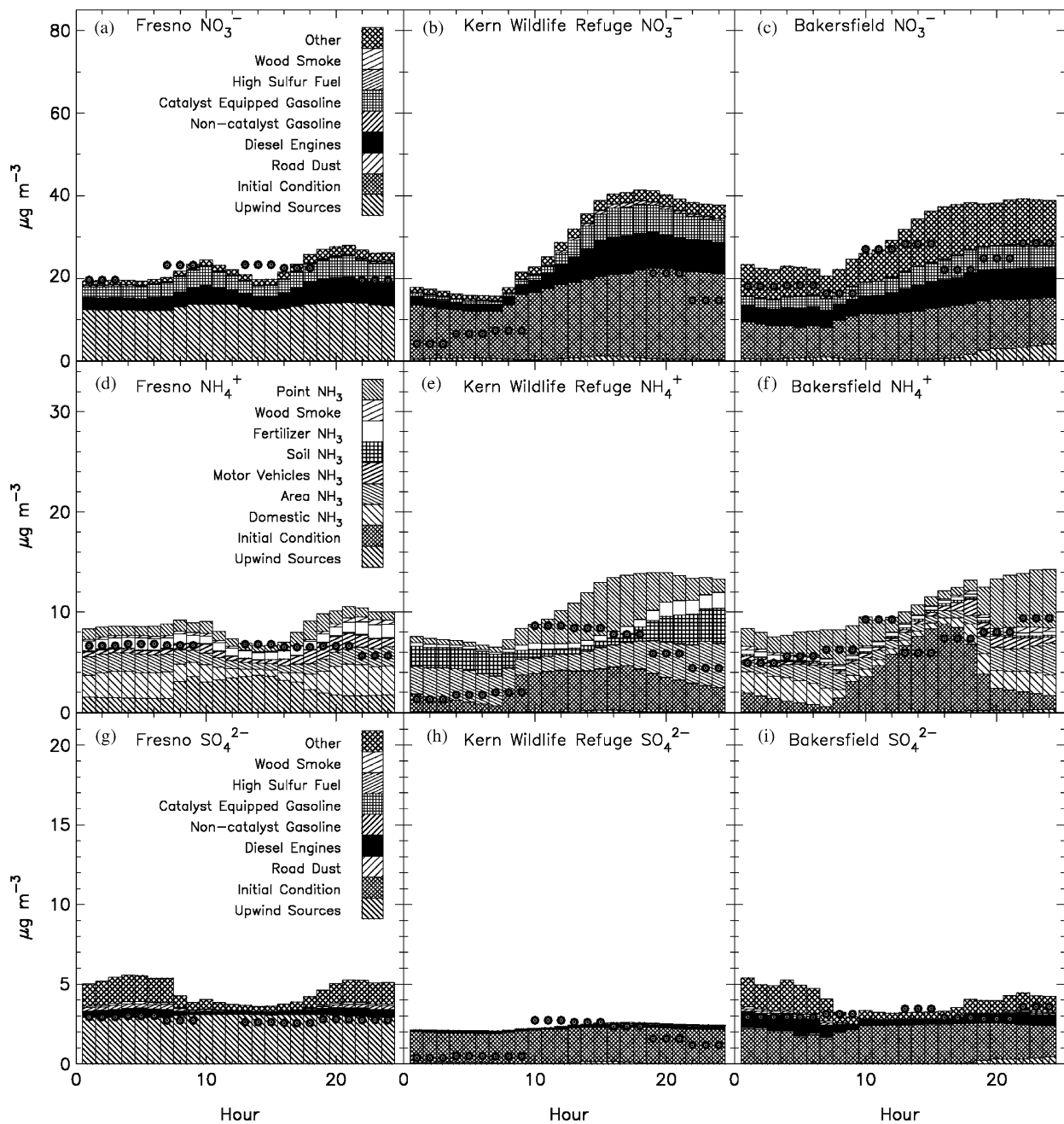


Fig. 3. Observed and predicted time series of PM<sub>2.5</sub> nitrate, sulfate and ammonium ion on 6 January 1996 for Fresno, Kern Wildlife Refuge and Bakersfield in the SJV.

Predictions agree well with the observations at the two urban sites for most of the hours. At the rural Kern Wildlife Refuge, model predictions are greater than measured concentrations during the early morning and late evening hours. The preliminary ammonia emissions inventory used in the current study may slightly over predict ammonia emissions

at some locations. Fig. 3(d) shows that the most significant contributors to secondary ammonium ion at Fresno are point sources, fertilizer application, area sources (including agriculture), and domestic sources. Upwind sources of ammonia (entered in the SJV as a boundary condition) also contribute significantly to PM<sub>2.5</sub> ammonium ion

concentrations at Fresno. Fig. 3(e) shows that  $\text{NH}_3$  emitted from soil and fertilizer application are significant contributors to  $\text{PM}_{2.5}$  ammonium ion concentrations at Kern Wildlife Refuge. The rural site is strongly affected by the gas phase ammonia and  $\text{PM}_{2.5}$  ammonium ion released from sources prior to 4 January 1996 (entered the SJV as an initial condition). Fig. 3(f) shows a similar pattern for ammonium ion concentrations at Bakersfield with slightly lower contributions from soil and fertilizer and greater contributions from domestic sources. Figs. 3(g)–(i) show the predicted and observed  $\text{PM}_{2.5}$  sulfate concentrations at Fresno, Kern Wildlife Refuge and Bakersfield, respectively. Both predicted and measured  $\text{PM}_{2.5}$  sulfate concentrations at all three sites are relatively constant at  $2\text{--}5\ \mu\text{g m}^{-3}$  during the entire day. Model calculations predict that the majority of the  $\text{PM}_{2.5}$  sulfate aerosol is associated with either upwind sources or initial conditions. Catalyst-equipped gasoline engines and diesel engines make minor

contributions to  $\text{PM}_{2.5}$  sulfate concentrations at all three sites.

Figs. 4(a)–(f) show the observed and predicted nitrate, ammonium ion and sulfate mass distributions for Riverside (15:00–19:00, 25 September 1996) and Bakersfield (11:00–14:00, 5 January 1996). Figs. 4(a)–(c) show the observed and predicted size distribution for nitrate, ammonium ion and sulfate at Riverside. Good agreement is generally observed between the model predictions and the measured concentrations. The predicted and observed maximum mass concentrations for nitrate, ammonium ion and sulfate are all in the size range of  $0.44\text{--}0.77\ \mu\text{m}$ . The model tends to slightly over-predict in the small size ranges and slightly under-predict for larger particles. Impactor measurements were not made above  $1.8\ \mu\text{m}$  particle diameter. Figs. 4(d)–(f) show the observed and predicted size distribution for nitrate, ammonium ion and sulfate at Bakersfield. Measurements made using cascade impactors were scaled to match  $\text{PM}_{10}$

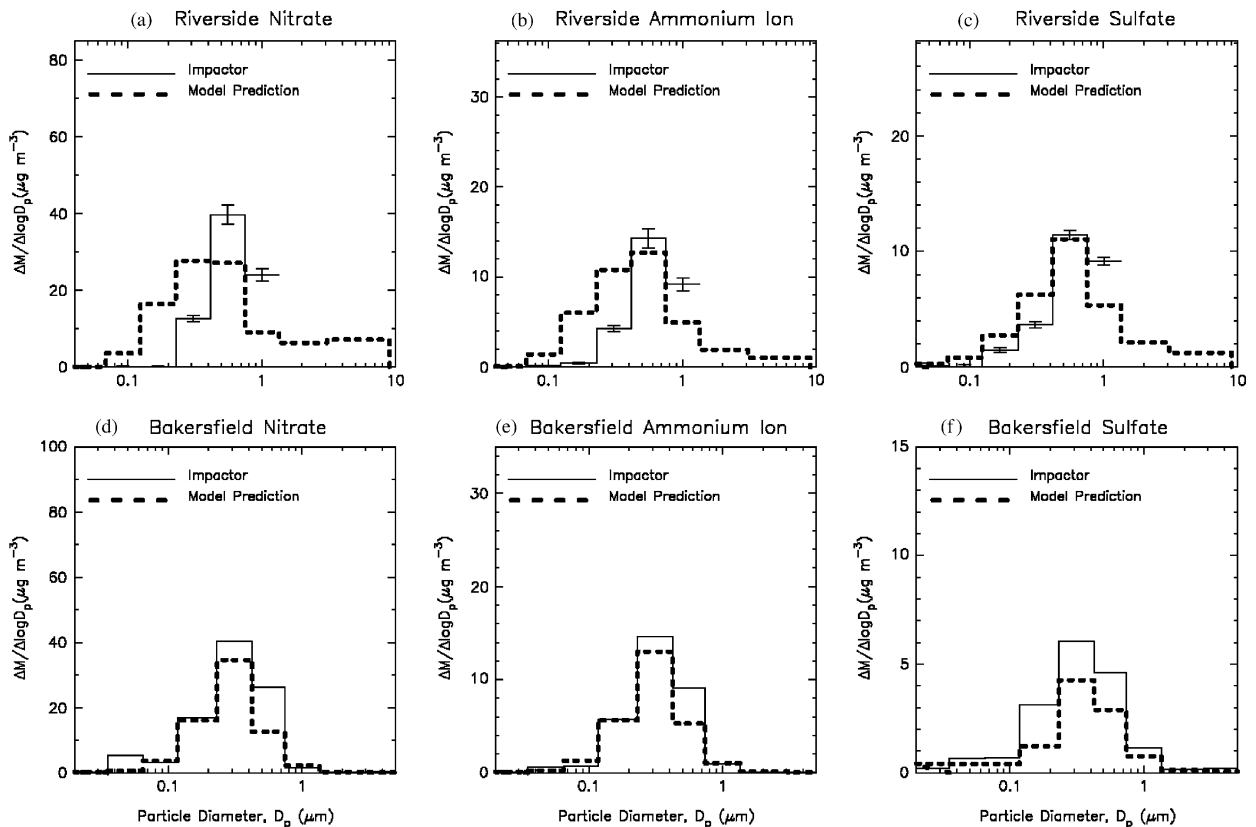


Fig. 4. Observed and predicted particle mass distributions as a function of particle size for Riverside (14:00–17:00, 25 September 1996) and Bakersfield (11:00–14:00, 6 January 1996).

measurements for each species (Held et al., 2004). Predicted nitrate, ammonium ion and sulfate size distributions show strong agreement with the measured size distributions. Both model predictions and measurements indicate that most of the secondary nitrate, ammonium ion and sulfate is in the size range of 0.1–1  $\mu\text{m}$  with the maximum concentration occurring in the size range of 0.25–0.44  $\mu\text{m}$ . Sulfate mass is slightly under predicted, but since overall sulfate concentrations are so small this discrepancy is not a major concern.

### 5.2. Regional source contributions to secondary particulate matter—SoCAB

Fig. 5(a) shows the regional distribution of the predicted 24-h average PM<sub>2.5</sub> nitrate concentration in the SoCAB on 25 September 1996. The peak PM<sub>2.5</sub> nitrate concentration of approximately 50  $\mu\text{g m}^{-3}$  is located in the northeastern portion of the air basin that is downwind of the major emission source of NO<sub>x</sub> in the Los Angeles area and the dairies located just west of Riverside. Figs. 5(b)–(g) show the regional distribution of the predicted 24-h average source contributions to PM<sub>2.5</sub> nitrate concentrations. All the sources except for the boundary condition contribute to the total PM<sub>2.5</sub> nitrate concentration most significantly in the northeastern portion of the air basin. In other areas of the domain, the NO<sub>x</sub> does not convert to PM<sub>2.5</sub> nitrate effectively because the partitioning of gas-phase nitric acid to the particle phase is limited by the amount of ammonia in the atmosphere. Figs. 5(b)–(c) show that diesel engines and catalyst equipped gasoline engines make similar contributions to PM<sub>2.5</sub> nitrate in the domain. The maximum PM<sub>2.5</sub> nitrate concentration associated with both of these sources is approximately 18  $\mu\text{g m}^{-3}$ . Fig. 5(d) shows that the spatial distribution of the predicted contribution from non-catalyst equipped gasoline engines to PM<sub>2.5</sub> nitrate is similar to the spatial distribution of nitrate from diesel engines and catalyst equipped gasoline engines but the relative contribution from non-catalyst equipped gasoline engines is much smaller (less than 2.5  $\mu\text{g m}^{-3}$ ). Fig. 5(e) shows that high-sulfur fuel combustion contributes approximately 2.5  $\mu\text{g m}^{-3}$  to predicted nitrate concentrations. Fig. 5(f) shows that other anthropogenic sources make a maximum contribution of 5  $\mu\text{g m}^{-3}$  to PM<sub>2.5</sub> nitrate concentrations. Fig. 5(g) shows that NO<sub>x</sub> from upwind sources (entered in the SoCAB as a boundary condition)

only contributes approximately 2  $\mu\text{g m}^{-3}$  to predicted PM<sub>2.5</sub> nitrate concentrations at inland locations.

Fig. 6(a) shows the regional distribution of the predicted 24-h average PM<sub>2.5</sub> ammonium ion concentration in the SoCAB on 25 September 1996. The maximum predicted PM<sub>2.5</sub> ammonium ion concentration of approximately 20  $\mu\text{g m}^{-3}$  is located in the northeastern portion of the air basin that is downwind of the Chino dairy area. Figs. 6(b)–(g) show the regional distribution of the predicted 24-h average source contributions to PM<sub>2.5</sub> ammonium ion concentrations. Fig. 6(b) shows that PM<sub>2.5</sub> ammonium ion concentrations are mainly associated with NH<sub>3</sub> emissions from animal sources located in the Chino dairy area west of Riverside. The maximum contribution associated with animal sources is approximately 14  $\mu\text{g m}^{-3}$ . Fig. 6(c) shows that ammonium ion formed from catalyst-equipped gasoline engine emissions is broadly distributed in the inland region of the air basin with a maximum concentration of approximately 2  $\mu\text{g m}^{-3}$ . Fig. 7(d) shows that the maximum concentration of ammonium ion from domestic ammonia sources is approximately 2  $\mu\text{g m}^{-3}$  downwind of central Los Angeles. Fig. 6(e) shows that ammonium ion associated with soil and fertilizer sources has a maximum concentration of approximately 1–2  $\mu\text{g m}^{-3}$  mainly located in the northern part of the air basin. Fig. 6(f) shows that the contribution to PM<sub>2.5</sub> ammonium ion from other anthropogenic sources is significant in the region near Long Beach and west of Riverside. The maximum contribution associated with this lumped source is approximately 6  $\mu\text{g m}^{-3}$ . Fig. 6(g) shows that the upwind sources of ammonium ion are predicted to be insignificant in the inland portion of the SoCAB. The maximum contribution associated with upwind sources is approximately 2–3  $\mu\text{g m}^{-3}$  along the west boundary of the model domain.

Fig. 7(a) shows the regional distribution of the predicted 24-h average PM<sub>2.5</sub> sulfate concentration in the SoCAB on 25 September 1996. The maximum concentration of approximately 13  $\mu\text{g m}^{-3}$  is located in the Long Beach area. An obvious plume of PM<sub>2.5</sub> sulfate with a concentration of approximately 7  $\mu\text{g m}^{-3}$  can be observed in the region downwind of Long Beach. The major sources that contribute to PM<sub>2.5</sub> sulfate are diesel engines, high-sulfur fuel combustion, other anthropogenic sources and sulfate sources upwind of the SoCAB. Fig. 7(b) shows that the contribution from diesel

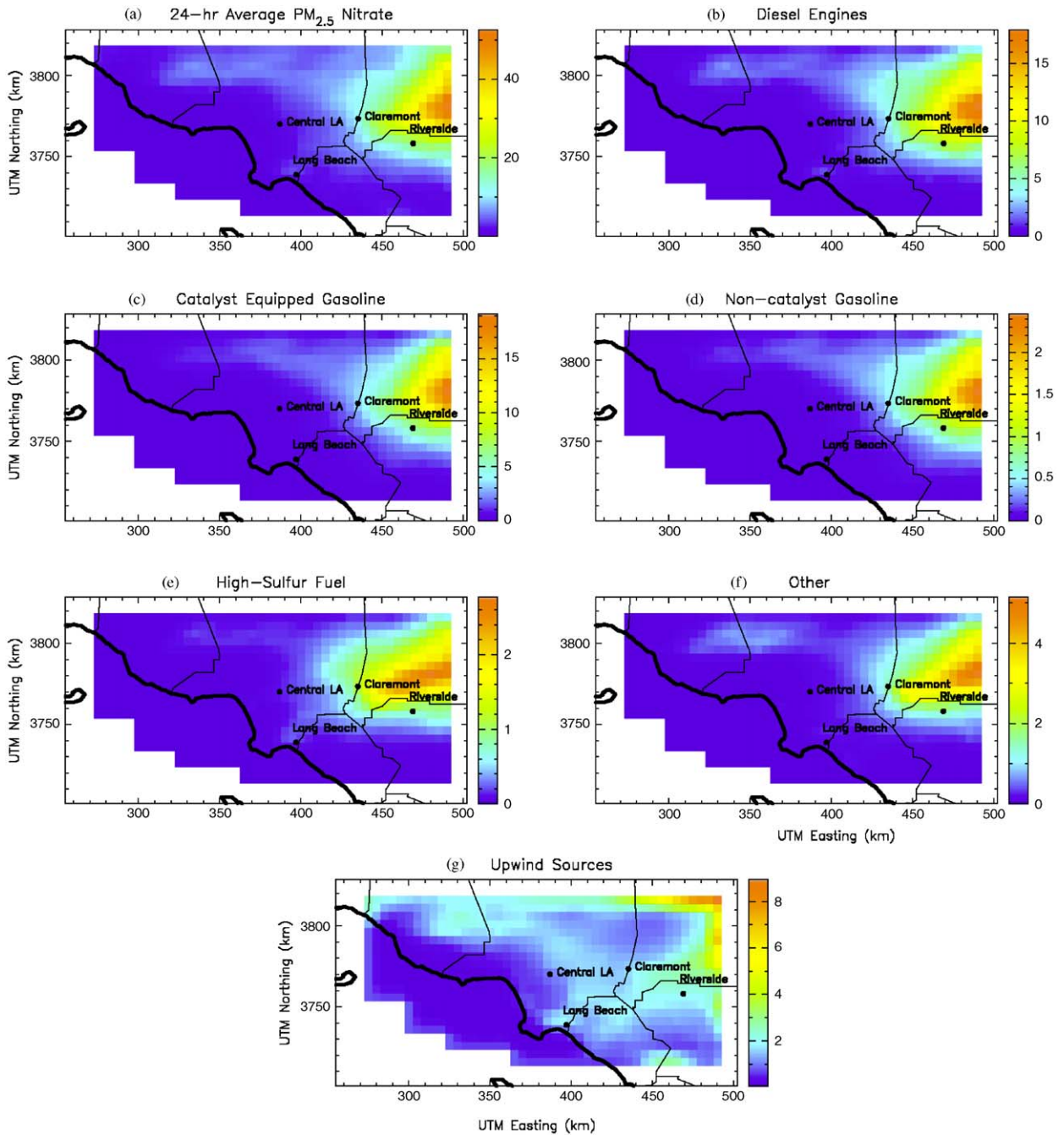


Fig. 5. Predicted regional source contribution to PM<sub>2.5</sub> nitrate in the SoCAB on 25 September 1996 (units are  $\mu\text{g m}^{-3}$ ). Note that the scales for each panel are different.

engines to predicted PM<sub>2.5</sub> sulfate concentrations is  $4.8 \mu\text{g m}^{-3}$  in the coastal areas of Long Beach. Fig. 7(c) shows that high-sulfur fuel combustion activities contribute as much as  $8 \mu\text{g m}^{-3}$  of PM<sub>2.5</sub> sulfate in the Long Beach area. Fig. 7(d) shows that other anthropogenic sources contribute approxi-

mately  $1 \mu\text{g m}^{-3}$  of PM<sub>2.5</sub> sulfate in the corridor between Long Beach area and Riverside. Fig. 7(e) shows that the PM<sub>2.5</sub> sulfate from sources upwind of the SoCAB is approximately  $4.8 \mu\text{g m}^{-3}$  over the ocean. This unknown source accounts for the majority of the fine-particle sulfate found in the SoCAB.

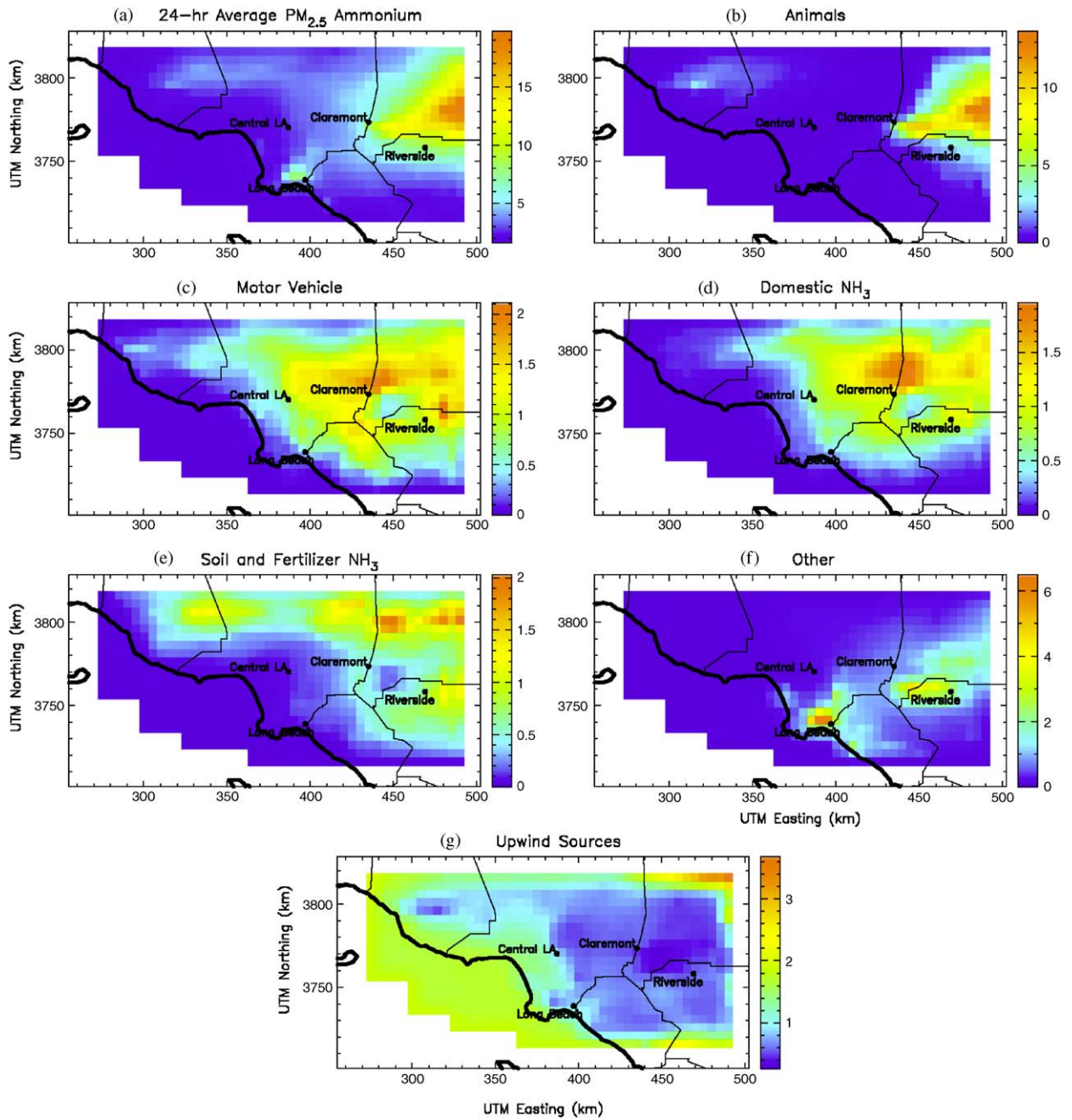


Fig. 6. Predicted regional source contribution to PM<sub>2.5</sub> ammonium ion in the SoCAB on 25 September 1996 (units are  $\mu\text{g m}^{-3}$ ). Note that the scales for each panel are different.

### 5.3. Regional source contributions to secondary particulate matter—SJV

Fig. 8(a) shows the predicted regional distribution of 24-h average PM<sub>2.5</sub> nitrate in the SJV on 6 January 1996. Concentrations range from approximately  $10\text{--}20\ \mu\text{g m}^{-3}$  along the edges of the moun-

tain boundaries to a maximum concentration of approximately  $48\ \mu\text{g m}^{-3}$  east of Kern Wildlife Refuge. Figs. 8(b)–(i) show the predicted regional distribution of 24-h average source contributions to PM<sub>2.5</sub> nitrate concentrations. Diesel engines and catalyst equipped gasoline engines are the two most important local sources that contribute to the

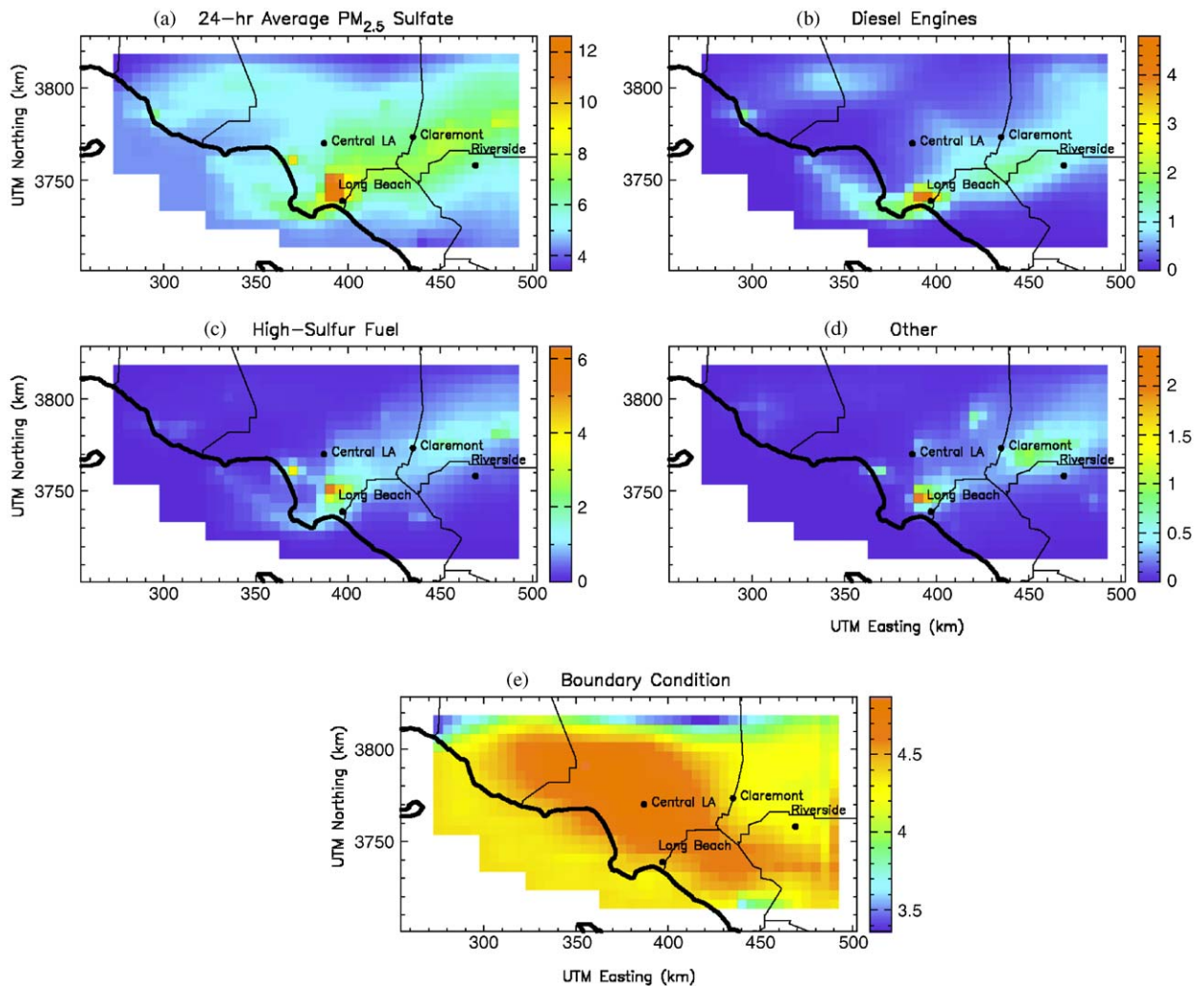


Fig. 7. Predicted regional source contribution to PM<sub>2.5</sub> sulfate in the SoCAB on 25 September 1996 (units are  $\mu\text{g m}^{-3}$ ). Note that the scales for each panel are different.

elevated secondary nitrate concentrations in the SJV. Fig. 8(b) and (c) show that PM<sub>2.5</sub> nitrate associated with diesel engines and catalyst equipped gasoline engines have similar spatial distributions with enhanced concentrations along the highway CA-99 corridor and a peak concentration northeast of Kern Wildlife Refuge. The maximum PM<sub>2.5</sub> nitrate concentrations from diesel engines and catalyst equipped gasoline engines are approximately 18 and  $14 \mu\text{g m}^{-3}$ , respectively. Fig. 8(d) shows that high-sulfur fuel combustion generally has low contribution to PM<sub>2.5</sub> nitrate in the SJV. Fig. 8(e) shows that the predicted spatial distribution of PM<sub>2.5</sub> nitrate associated with non-catalyst gasoline engines is similar to the spatial distribution of nitrate associated with diesel engines and catalyst

equipped gasoline engines, but the maximum concentration associated with non-catalyst gasoline engines is only  $0.3 \mu\text{g m}^{-3}$ . Wood smoke also makes a minor contribution to predicted nitrate concentrations with a peak value of  $0.8 \mu\text{g m}^{-3}$  near Fresno. Fig. 8(g) shows that other anthropogenic sources contribute  $9 \mu\text{g m}^{-3}$  to PM<sub>2.5</sub> nitrate in the Bakersfield area. Fig. 8(h) shows that the upwind sources of NO<sub>x</sub> (entered in the SJV as a boundary condition) contribute approximately  $20 \mu\text{g m}^{-3}$  of PM<sub>2.5</sub> nitrate along the north edge of the modeling domain. The southern part of the model region is not heavily influenced by upwind sources because advection patterns do not transport material this far south during the 3-day simulated period. Nitrate and its precursor species released from sources prior

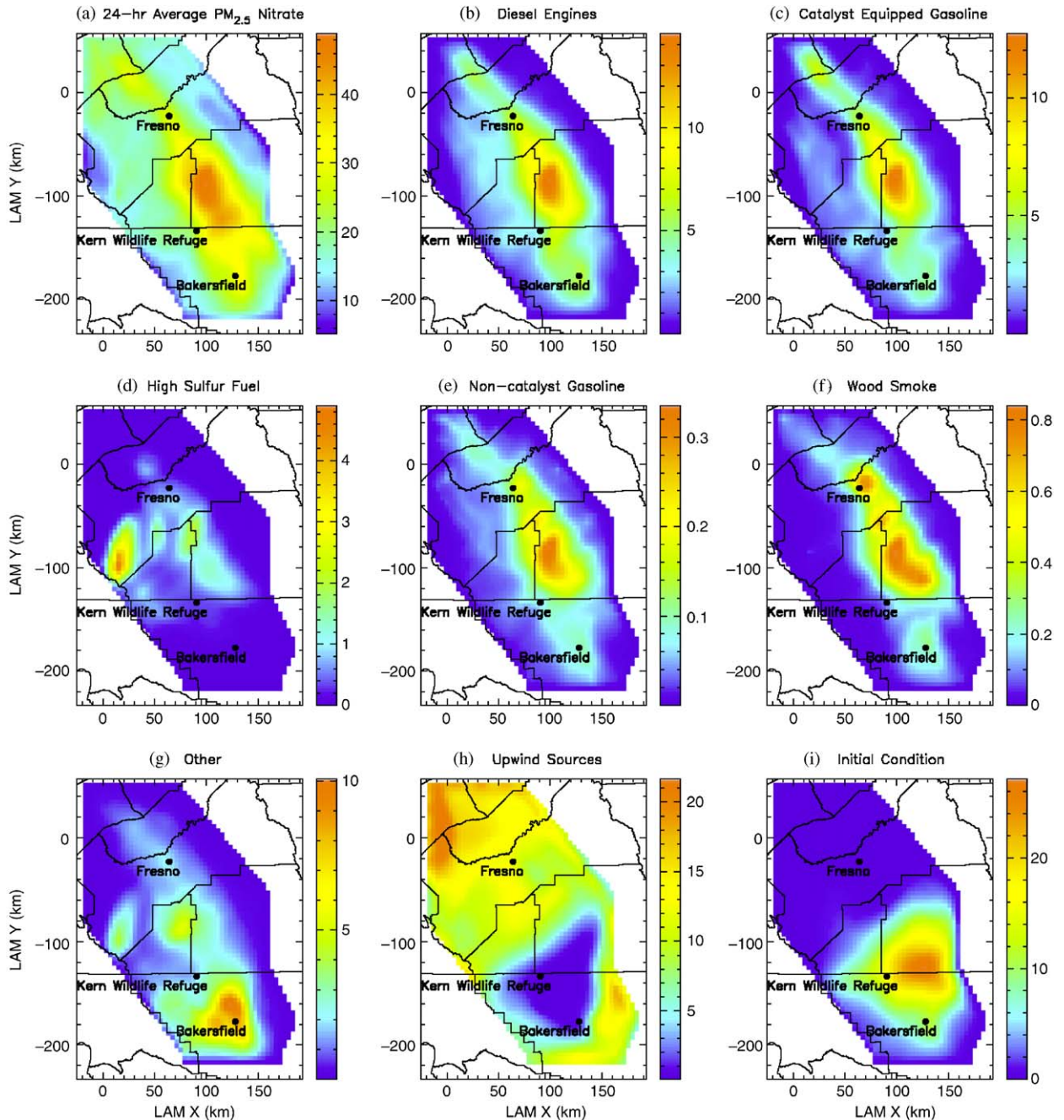


Fig. 8. Predicted regional source contribution to PM<sub>2.5</sub> nitrate in the SJV on 6 January 1996 (units are  $\mu\text{g m}^{-3}$ ). Note that the scales for each panel are different.

to 4 January 1996 (entered in the SJV as an initial condition) contribute approximately  $26 \mu\text{g m}^{-3}$  of PM<sub>2.5</sub> nitrate in the area east of Kern Wildlife Refuge and north of Bakersfield.

Fig. 9(a) shows the predicted regional distribution of 24-h average PM<sub>2.5</sub> ammonium ion concentra-

tions in the SJV on 6 January 1996. Concentrations range from approximately  $5\text{--}7 \mu\text{g m}^{-3}$  along the edges of the mountain boundaries to a maximum concentration of approximately  $15 \mu\text{g m}^{-3}$  northwest of Bakersfield. Figs. 9(b)–(i) show the regional distribution of predicted 24-h average

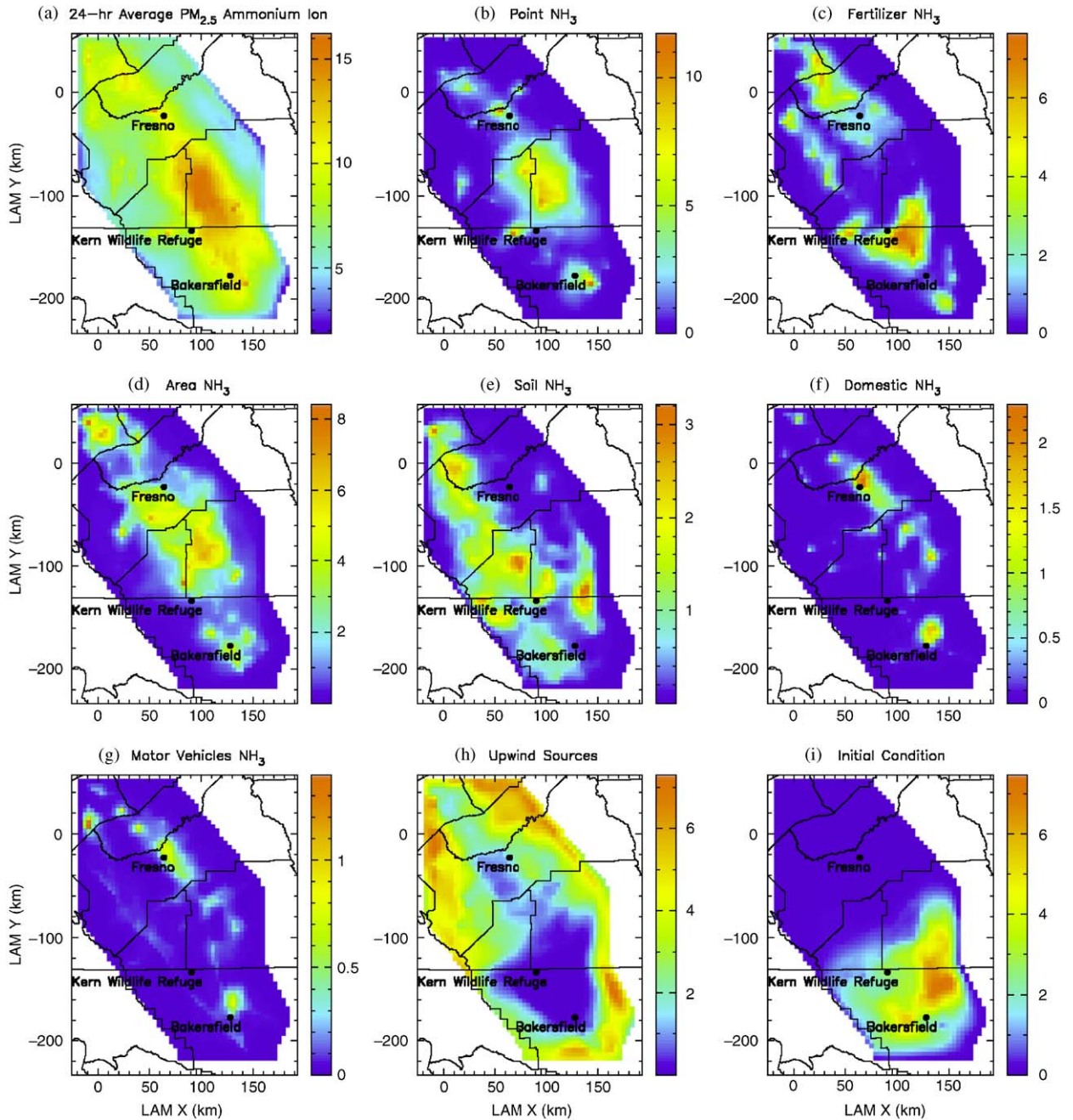


Fig. 9. Predicted regional source contribution to PM<sub>2.5</sub> ammonium ion in the SJV on 6 January 1996 (units are  $\mu\text{g m}^{-3}$ ). Note that the scales for each panel are different.

source contributions to PM<sub>2.5</sub> ammonium ion concentrations in the SJV. Point NH<sub>3</sub>, fertilizer NH<sub>3</sub>, area NH<sub>3</sub> (including agriculture) and soil NH<sub>3</sub> are the most important local sources that contribute to the ammonium ion concentration. Point NH<sub>3</sub> sources produce a maximum ammonium ion con-

centration of approximately  $8.5 \mu\text{g m}^{-3}$  north of Kern Wildlife Refuge. Fertilizer NH<sub>3</sub> contributes approximately  $7 \mu\text{g m}^{-3}$  of ammonium ion between Bakersfield and Kern Wildlife Refuge. Area NH<sub>3</sub> sources have a broader regional distribution with a maximum contribution of approximately  $6 \mu\text{g m}^{-3}$

between Fresno and Kern Wildlife Refuge. Soil  $\text{NH}_3$  has a maximum  $\text{PM}_{2.5}$  ammonium ion contribution of  $2.8 \mu\text{g m}^{-3}$  primarily along the Coastal Range that forms the western boundary of the modeling domain. Domestic  $\text{NH}_3$  sources and motor vehicle  $\text{NH}_3$  sources have a maximum contribution in the Fresno area of 2 and  $0.7 \mu\text{g m}^{-3}$ , respectively. The mass concentration due to these two sources is only significant near the urban areas along the Interstate I-5 and highway CA-99. Ammonia released from upwind sources (entered in the SJV as a boundary condition) contributes  $6 \mu\text{g m}^{-3}$  to predicted  $\text{PM}_{2.5}$  ammonium ion concentrations near the north and upper-west edge of the modeling domain. Ammonia released from sources prior to 4 January 1996 (entered in the SJV as an initial condition) contributes approximately  $7 \mu\text{g m}^{-3}$  to predicted  $\text{PM}_{2.5}$  ammonium ion concentrations in the southern end of the modeling domain northeast of Bakersfield.

Fig. 10(a) shows the predicted regional distribution of 24-h average  $\text{PM}_{2.5}$  sulfate in the SJV on 6 January 1996. The predicted  $\text{PM}_{2.5}$  sulfate concentration is only  $2\text{--}3 \mu\text{g m}^{-3}$  for most of the SJV with slightly high concentrations of approximately  $4 \mu\text{g m}^{-3}$  near Fresno and Bakersfield. The highest concentration of approximately  $8.5 \mu\text{g m}^{-3}$  is located near the western end of Fresno County. Figs. 10(b)–(h) show the regional distribution of the predicted 24-h average source contributions to  $\text{PM}_{2.5}$  sulfate concentrations. Fig. 10(b) shows that high-sulfur fuel combustion activities contribute  $5\text{--}6 \mu\text{g m}^{-3}$  of fine-particle sulfate, producing the peak  $\text{PM}_{2.5}$  sulfate concentration predicted in the western end of Fresno County. Figs. 10(c)–(e) show that the transportation sources of sulfate (diesel engines, catalyst equipped engines and non-catalyst gasoline engines) are most significant in the urban areas of Fresno and Bakersfield and along Interstate I-5 and highway CA-99. Only diesel engines (maximum concentration approximately  $0.8 \mu\text{g m}^{-3}$ ) are predicted to make a significant contribution to  $\text{PM}_{2.5}$  sulfate. Catalyst and non-catalyst gasoline engines are predicted to contribute less than  $0.1 \mu\text{g m}^{-3}$  to the  $\text{PM}_{2.5}$  sulfate. Fig. 10(f) shows that other anthropogenic sources contribute approximately  $1\text{--}2 \mu\text{g m}^{-3}$  of  $\text{PM}_{2.5}$  sulfate in the Fresno and Bakersfield areas. Fig. 10(g) shows that the northern part of the study domain is dominated by upwind sources (entered in the SJV as a boundary condition) with a relatively uniform concentration of approximately  $3 \mu\text{g m}^{-3}$ . Fig. 10(h)

shows that sulfate aerosol produced before 4 January 1996 (entered in the SJV as an initial condition) contributes approximately  $3 \mu\text{g m}^{-3}$  of  $\text{PM}_{2.5}$  sulfate in the lower part of the SJV on 6 January 1996.

#### 5.4. Domain-averaged source contribution to secondary particulate matter

Table 1 shows the domain-averaged source contributions to predicted secondary nitrate, sulfate and ammonium ion concentrations in the SoCAB on 25 September 1996. The areas over the ocean are not included in the averaging process. The average nitrate ammonium ion and sulfate concentrations are 8.5, 4.8 and  $5.6 \mu\text{g m}^{-3}$ , respectively. Transportation related sources dominate the predicted formation of secondary  $\text{PM}_{2.5}$  nitrate in the SoCAB. Diesel engines and catalyst equipped gasoline engines account for 34.6% and 28.1% of the predicted  $\text{PM}_{2.5}$  nitrate concentration, respectively. Predicted ammonium ion concentrations in the SoCAB are mainly associated with animal sources (28.2%), catalyst equipped gasoline engines (16.2%) and other anthropogenic sources (13.1%). The majority of the  $\text{PM}_{2.5}$  sulfate in the SoCAB (77.5%) is associated with upwind sources with smaller contributions from diesel engines (10.5%) and high-sulfur fuel combustion (7.6%).

Table 2 shows the domain-averaged source contributions to predicted secondary nitrate, ammonium ion and sulfate concentrations in the SJV on 6 January 1996. The averaged nitrate, ammonium ion and sulfate concentrations are 20.9, 7.9, and  $2.7 \mu\text{g m}^{-3}$ , respectively. Approximately 13% of the ammonium ion and 20% of the nitrate and sulfate are associated with emissions released prior to 4 January 1996 (represented in the model calculations as an initial condition). The source of this material cannot be identified in the current study, but it would be reasonable to assume that this older particulate matter was formed by the same sources and mechanisms that generate fresh secondary particulate matter between 4–6 January 1996. The adjusted relative contributions from other sources have been calculated making this assumption and are shown in Table 2. 45.2–57% of the  $\text{PM}_{2.5}$  nitrate, 34–39.4% of the  $\text{PM}_{2.5}$  ammonium ion and 65.7–83.1% of the  $\text{PM}_{2.5}$  sulfate in the current study is associated with emissions from upwind sources that are outside of the SJV. In terms of local sources (sources within the SJV), diesel

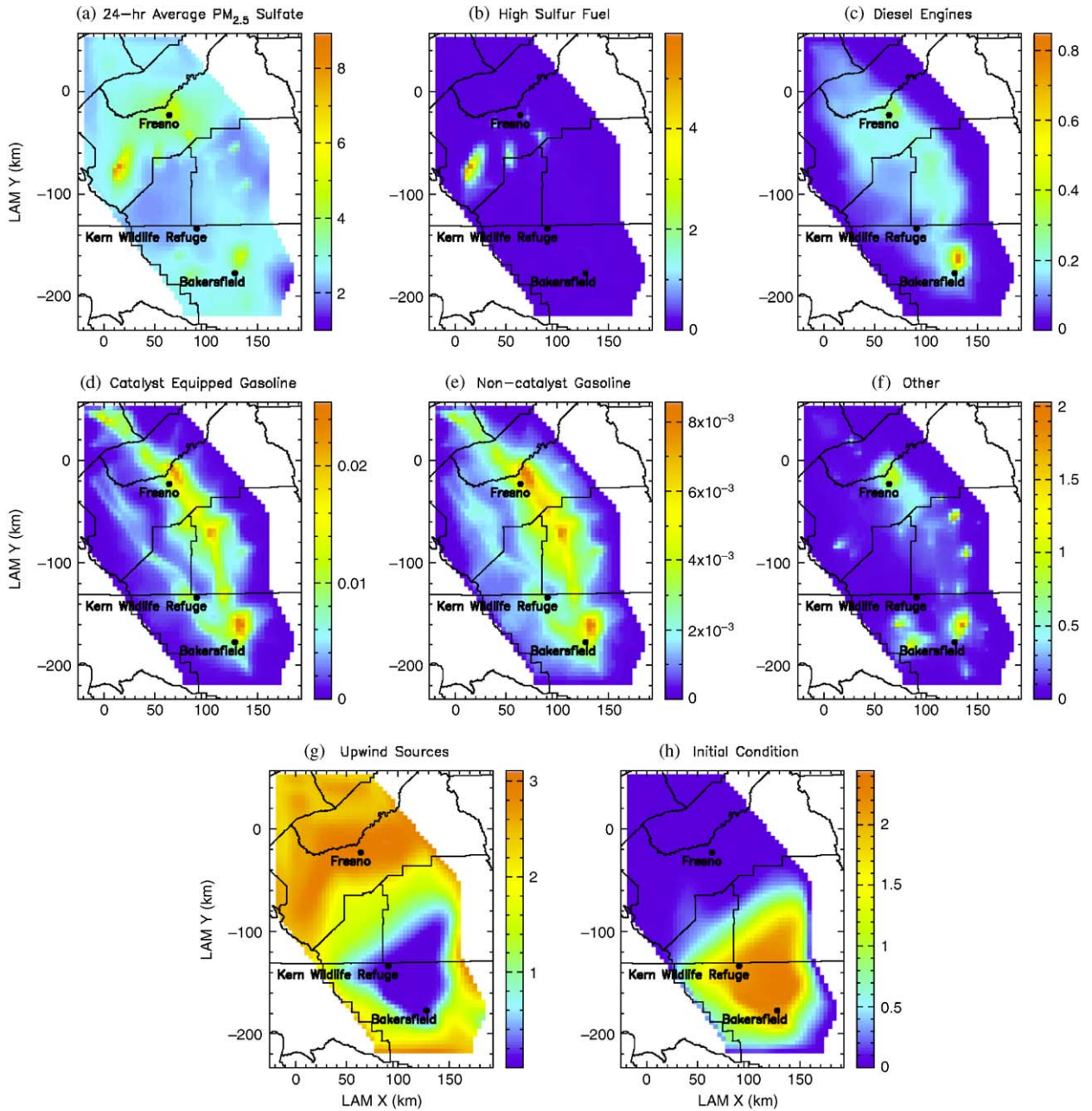


Fig. 10. Predicted regional source contribution to PM<sub>2.5</sub> sulfate in the SJV on 6 January 1996 (units are  $\mu\text{g m}^{-3}$ ). Note that the scales for each panel are different.

engines (13.5–17.0%) and catalyst equipped gasoline engines (10.2–12.8%) are the two most significant local contributors to PM<sub>2.5</sub> nitrate. Area NH<sub>3</sub> (16.7–25.3%), point NH<sub>3</sub> (14.3–21.7%), fertilizer NH<sub>3</sub> (11.4–17.3%) and soil NH<sub>3</sub> (7.2–10.9%) are the most important local sources of PM<sub>2.5</sub> ammonium ion in the SJV. High-sulfur fuel combustion (3.6–4.7%) and diesel engines

(3.1–4.0%) are the two largest local contributors to PM<sub>2.5</sub> sulfate.

### 6. Uncertainty analysis

The uncertainties in the surface pollutant concentrations and source attribution in the SJV domain due to uncertainties in the model input

Table 1  
Domain-averaged source contributions to secondary PM<sub>2.5</sub> in the SoCAB on 25 September 1996

Source category	Nitrate		Ammonium ion		Sulfate	
	$\mu\text{g m}^{-3}$	%	$\mu\text{g m}^{-3}$	%	$\mu\text{g m}^{-3}$	%
Crustal material	0.01	0.1	0.00	0.0	0.00	0.0
Paved road dust	0.02	0.3	0.00	0.0	0.04	0.7
Diesel engines	2.93	34.6	0.00	0.0	0.58	10.5
Meat cooking	0.03	0.3	0.00	0.0	0.01	0.1
Non-catalyst gasoline	0.40	4.7	0.00	0.0	0.02	0.3
Catalyst equipped gasoline	2.38	28.1	0.78	16.2	0.03	0.5
High-sulfur fuel	0.52	6.2	0.00	0.0	0.42	7.6
Refrigerant losses	0.00	0.0	0.01	0.2	0.00	0.0
Domestic NH <sub>3</sub>	0.00	0.0	0.61	12.8	0.00	0.0
Animal NH <sub>3</sub>	0.00	0.0	1.36	28.2	0.00	0.0
Soil and fertilizer NH <sub>3</sub>	0.00	0.0	0.56	11.6	0.00	0.0
Other anthropogenic sources	0.76	9.0	0.63	13.1	0.15	2.7
Upwind sources	1.42	16.7	0.86	17.9	4.30	77.5
Total	8.5	100.0	4.8	100.0	5.6	100.0

Table 2  
Domain-averaged source contributions to secondary PM<sub>2.5</sub> in the SJV on 6 January 1996

Source category	Nitrate <sup>a</sup>			Ammonium ion <sup>a</sup>			Sulfate <sup>a</sup>		
	$\mu\text{g m}^{-3}$	%		$\mu\text{g m}^{-3}$	%		$\mu\text{g m}^{-3}$	%	
Road dust	0.05	0.2%	(0.3)	0.00	0.0%	(0.0)	0.02	0.7%	(0.9)
Diesel engines	2.80	13.5%	(17.0)	0.00	0.0%	(0.0)	0.08	3.1%	(4.0)
Non-catalyst gasoline	0.06	0.3%	(0.4)	0.00	0.0%	(0.0)	0.00	0.1%	(0.1)
Catalyst equipped gasoline	2.12	10.2%	(12.8)	0.07	0.8%	(1.3)	0.00	0.1%	(0.2)
Meat cooking	0.01	0.1%	(0.1)	0.00	0.1%	(0.1)	0.00	0.0%	(0.0)
High-sulfur fuel	0.35	1.7%	(2.1)	0.00	0.0%	(0.0)	0.10	3.6%	(4.7)
Wood smoke	0.14	0.7%	(0.8)	0.03	0.4%	(0.6)	0.01	0.3%	(0.4)
Domestic NH <sub>3</sub>	0.00	0.0%	(0.0)	0.10	1.3%	(2.0)	0.00	0.0%	(0.0)
Area NH <sub>3</sub>	0.00	0.0%	(0.0)	1.32	16.7%	(25.3)	0.00	0.0%	(0.0)
Soil NH <sub>3</sub>	0.00	0.0%	(0.0)	0.57	7.2%	(10.9)	0.00	0.0%	(0.0)
Fertilizer NH <sub>3</sub>	0.00	0.0%	(0.0)	0.90	11.4%	(17.3)	0.00	0.0%	(0.0)
Point NH <sub>3</sub>	0.00	0.0%	(0.0)	1.13	14.3%	(21.7)	0.00	0.0%	(0.0)
Other anthropogenic sources	1.58	7.6%	(9.5)	0.00	0.0%	(0.0)	0.12	4.4%	(5.7)
Initial condition	4.32	20.7%	(0.0)	2.68	13.7%	(0.0)	0.59	22.0%	(0.0)
Upwind sources	9.42	45.2%	(57.0)	1.08	34.0%	(39.4)	1.78	65.7%	(84.1)
Total	20.9	100.0%	(100.0)	7.9	100.0%	(100.0)	2.7	100.0%	(100.0)

<sup>a</sup>Values in parenthesis assume that the initial condition is distributed according to the pattern established during the 3-day simulation.

emissions and meteorological fields were studied by randomly perturbing the inputs using a Monte Carlo simulation. Measured surface and upper level wind speeds and directions were randomly perturbed to generate multiple wind fields for each hour. It was assumed that the accuracy of wind speed observations in the surface layer was  $\pm 1.5\%$  (typical accuracy of wind vanes) and in the upper

layer was  $\pm 1.0\text{ m/s}$  (typical accuracy of wind profilers). The accuracy of the wind direction observation in the surface layer was assumed to be  $\pm 5^\circ$  (typical accuracy of wind vane) and in the upper layer was  $\pm 10^\circ$  (typical accuracy of wind profilers). Temperature, relative humidity, and mixing height were also perturbed in these studies by assuming that the actual values for these

meteorology variables were normally distributed about the measured value with a standard error of 30%. Random perturbations of the gas and PM emissions were carried out by assuming that the actual emissions rate for each source was normally distributed about the nominal inventory value with a standard error of 30%. A total of 30 simulations were performed using various combinations of perturbed input fields. The maximum uncertainties in the SJV domain were found to be 3, 0.3 and  $0.9 \mu\text{g m}^{-3}$  for 24-h average PM<sub>2.5</sub> nitrate, sulfate and ammonium ion concentrations. The maximum relative uncertainty (standard deviation at each grid cell divided by the mean value for that grid cell) in the SJV domain for the 24-h average PM<sub>2.5</sub> nitrate, sulfate and ammonium ion concentrations calculated from the 30 perturbation runs were found to be approximately 11%, 5% and 9.5%, respectively. The maximum relative uncertainties for 24-h average total, primary and secondary PM<sub>2.5</sub> in the SJV were 8.5%, 13% and 10%, respectively. The maximum of both absolute and relative uncertainty occurred in the region close to Bakersfield.

The uncertainties in the predicted surface pollutant concentrations in the SoCAB domain on 23–25 September 1996 due to uncertainties in the model input emission and meteorological fields have been previously studied using a similar Monte Carlo technique (Kleeman and Cass, 2001). Thirty air parcel trajectories ending at Riverside were generated by randomly perturbing the measured wind fields. Other meteorology variables and emissions were perturbed by assuming that the actual values were normally distributed about the nominal value with a standard error of 30%. The results of this analysis predict that the relative uncertainty in the calculated 24-h average total and primary PM<sub>2.5</sub> concentrations at Riverside on 25 September 1996 is 25% and 19%, respectively.

In summary, the uncertainties in the predicted total, primary and secondary PM<sub>2.5</sub> concentrations in the SJV and the SoCAB are on the order of 8.5–25%. This level of uncertainty is considered to be reasonable for an initial evaluation of source contributions to regional secondary particulate matter concentrations.

## 7. Conclusions

The analysis performed in the previous sections shows that secondary particulate matter formation

in two of the most heavily polluted air basins in the United States (SJV and SoCAB) is associated with a large number of diverse sources. Reductions in precursor gas emissions ( $\text{NO}_x$ ,  $\text{NH}_3$ , VOC,  $\text{SO}_x$ ) will be needed to reduce secondary particulate matter concentrations. The majority of the secondary particulate matter formed in the SoCAB is released from sources within that region, suggesting that a local control strategy may be effective. In contrast, the majority of the secondary particulate matter that forms in the SJV is associated with emissions from upwind areas, suggesting that more regional controls are needed. A larger study of particulate air quality is currently underway as a part of the California Regional Particulate Air Quality Study (CRPAQS) (Solomon and Magliano, 1999). Future modeling exercises will identify the upwind sources that contribute to the formation of secondary particulate matter in the SJV.

## Acknowledgements

This research was supported by the San Joaquin Valleywide Air Pollution Study Agency and the California Air Resources Board under contract #2000-05PM. Further support was provided by the Environmental Protection Agency Science To Achieve Results (STAR) program under Grant no. RD831082.

## References

- Chow, J.C., et al., 1992. Pm10 source apportionment in California San-Joaquin valley. *Atmospheric Environment Part a-General Topics* 26 (18), 3335–3354.
- Christoforou, C.S., Salmon, L.G., Hannigan, M.P., Solomon, P.A., Cass, G.R., 2000. Trends in fine particle concentration and chemical composition in Southern California. *Journal of the Air & Waste Management Association* 50 (1), 43–53.
- Dickerson, R.R., et al., 1997. The impact of aerosols on solar ultraviolet radiation and photochemical smog. *Science* 278 (5339), 827–830.
- Dreher, K.L., Costa, D.L., 2002. Systemic health effects of ambient air particulate matter exposure—preface. *Journal of Toxicology and Environmental Health-Part A* 65 (20), 1491–1492.
- Eldering, A., Cass, G.R., 1996. Source-oriented model for air pollutant effects on visibility. *Journal of Geophysical Research-Atmospheres* 101 (D14), 19343–19369.
- EPA, 2003a. Latest Findings on National Air Quality: 2002 Status and Trends Report, US EPA.
- EPA, 2003b. National Air Quality and Emissions Trends Report, 2003, US EPA.

- Griffing, G.W., 1980. Relations between the prevailing visibility, nephelometer scattering coefficient and sun-photometer turbidity coefficient. *Atmospheric Environment* 14 (5), 577–584.
- Held, A.E., Ying, Q., Kleeman, M.J., Schauer, J.J., Fraser, M.P., 2005. A comparison of the UCD/CIT air quality model and the CMB source-receptor model for primary airborne particulate matter. *Atmospheric Environment* 39 (12), 2281–2297.
- Held, T., Ying, Q., Kaduwela, A., Kleeman, M., 2004. Modeling particulate matter in the San Joaquin Valley with a source-oriented externally mixed three-dimensional photochemical grid model. *Atmospheric Environment* 38 (22), 3689–3711.
- Herner, J.D., Aw, J., Gao, O., Chang, P.J., Kleeman, M.J., 2005. Size and composition distribution of airborne particulate matter in Northern California: I—particulate mass, carbon, and water-soluble ions. *Air and Waste Management Association* 55, 30–51.
- Hughes, L.S., et al., 1999. Size and composition distribution of atmospheric particles in southern California. *Environmental Science & Technology* 33 (20), 3506–3515.
- Jacobson, M.Z., 2000. A physically based treatment of elemental carbon optics: implications for global direct forcing of aerosols. *Geophysical Research Letters* 27 (2), 217–220.
- Kleeman, M.J., Cass, G.R., 2001. A 3D Eulerian source-oriented model for an externally mixed aerosol. *Environmental Science & Technology* 35 (24), 4834–4848.
- Kleeman, M.J., Cass, G.R., Eldering, A., 1997. Modeling the airborne particle complex as a source-oriented external mixture. *Journal of Geophysical Research-Atmospheres* 102 (D17), 21355–21372.
- Lesins, G., Chylek, P., Lohmann, U., 2002. A study of internal and external mixing scenarios and its effect on aerosol optical properties and direct radiative forcing. *Journal of Geophysical Research-Atmospheres* 107(D10), art. no. 4094.
- Magliano, K.L., et al., 1999. Spatial and temporal variations in PM10 and PM2.5 source contributions and comparison to emissions during the 1995 integrated monitoring study. *Atmospheric Environment* 33 (29), 4757–4773.
- Mysliwicz, M.J., Kleeman, M.J., 2002. Source apportionment of secondary airborne particulate matter in a polluted atmosphere. *Environmental Science & Technology* 36 (24), 5376–5384.
- Neiburger, M., 1995. Visibility trends in Los Angeles. Report 11, Air Pollution Foundation, Los Angeles, CA.
- Ozkaynak, H., et al., 1996. Personal exposure to airborne particles and metals: results from the particle team study in riverside, California. *Journal of Exposure Analysis and Environmental Epidemiology* 6 (1), 57–78.
- Pilinis, C., 1989. Numerical-simulation of visibility degradation due to particulate matter—model development and evaluation. *Journal of Geophysical Research-Atmospheres* 94 (D7), 9937–9946.
- Pun, B.K., Seigneur, C., 2001. Sensitivity of particulate matter nitrate formation to precursor emissions in the California San Joaquin Valley. *Environmental Science & Technology* 35 (14), 2979–2987.
- Richards, L.W., et al., 1999. Optical properties of the San Joaquin valley aerosol collected during the 1995 integrated monitoring study. *Atmospheric Environment* 33 (29), 4787–4795.
- Schauer, J.J., Rogge, W.F., Hildemann, L.M., Mazurek, M.A., Cass, G.R., 1996. Source apportionment of airborne particulate matter using organic compounds as tracers. *Atmospheric Environment* 30 (22), 3837–3855.
- Solomon, P.A., Magliano, K.L., 1999. The 1995-integrated monitoring study (IMS95) of the California regional PM10/PM2.5 air quality study (CRPAQS): study overview. *Atmospheric Environment* 33 (29), 4747–4756.
- Stockwell, W.R., Watson, J.G., Robinson, N.F., Steiner, W., Sylte, W.W., 2000. The ammonium nitrate particle equivalent of NO<sub>x</sub> emissions for wintertime conditions in Central California's San Joaquin Valley. *Atmospheric Environment* 34 (27), 4711–4717.
- Watson, J.G., Chow, J.C., 2002. A wintertime PM2.5 episode at the Fresno, CA, supersite. *Atmospheric Environment* 36 (3), 465–475.
- Watson, J.G., et al., 1994. Chemical mass-balance source apportionment of Pm(10) during the Southern California air-quality study. *Aerosol Science and Technology* 21 (1), 1–36.
- Watson, J.G., et al., 2002a. Simulating changes in source profiles from coal-fired power stations: use in chemical mass balance of PM2.5 in the Mount Zirkel wilderness. *Energy & Fuels* 16 (2), 311–324.
- Watson, J.G., et al., 2002b. Receptor modeling application framework for particle source apportionment. *Chemosphere* 49 (9), 1093–1136.
- Ying, Q., Kleeman, M.J., 2003. Effects of aerosol UV extinction on the formation of ozone and secondary particulate matter. *Atmospheric Environment* 37 (36), 5047–5068.
- Ying, Q., Mysliwicz, M., Kleeman, M.J., 2004. Source apportionment of visibility impairment using a three-dimensional source-oriented air quality model. *Environmental Science & Technology* 38 (4), 1089–1101.